Article

Microelectrode Implantation in Human Insula: Technical Challenges and Recording Insights

Daphné Citherlet , Sami Heymann , Maya Aderka , Katarzyna Jurewicz , B. Suresh Krishna , Manon Robert , Alain Bouthillier , Olivier Boucher , Dang Khoa Nguyen [*]

Article

Microelectrode Implantation in Human Insula: Technical Challenges and Recording Insights

Daphné Citherlet [1,2,†], **Sami Heymann** [3,†], **Maya Aderka** [1,4], **Katarzyna Jurewicz** [4],
B. Suresh Krishna [4], **Manon Robert** [1], **Alain Bouthillier** [3], **Olivier Boucher** [1,5,‡]
and Dang Khoa Nguyen [1,2,6,‡,*]

[1] Neurosciences Axis, Centre de Recherche du Centre Hospitalier de l'Université de Montréal (CRCHUM), Montreal, QC, Canada
[2] Department of Neurosciences, Université de Montréal, Montréal, QC, Canada
[3] Neurosurgery Division, Centre Hospitalier de l'Université de Montréal (CHUM), Montreal, QC, Canada
[4] Department of Physiology, McGill University, Montreal, QC, Canada
[5] Department of Psychology, Université de Montréal, Montréal, QC, Canada
[6] Neurology Division, Centre Hospitalier de l'Université de Montréal (CHUM), Montreal, QC, Canada
[*] Correspondence: d.nguyen@umontreal.ca
[†] Co-first authors.
[††] Co-senior authors.

Abstract: Background/Objectives: Intracranial macroelectrode implantation is a pivotal clinical tool in the evaluation of drug-resistant epilepsy, allowing further insights into the localization of the epileptogenic zone and the delineation of eloquent cortical regions through cortical stimulation. Additionally, it provides an avenue to study brain functions by analyzing cerebral responses during neuropsychological paradigms. By combining macroelectrodes with *micro*electrodes, which allow to record the activity of individual neurons or smaller neural clusters, recordings could provide deeper insights into neuronal microcircuits and the brain's transitions in epilepsy and contribute to a better understanding of neuropsychological functions. In this study, one or two hybrid macro-micro electrodes were implanted in the anterior-inferior insular region in patients with refractory epilepsy. We report our experience and share some preliminary results; we also provide some recommendations regarding the implantation procedure of hybrid electrodes in the insular cortex. **Methods**: Stereoelectroencephalography was performed in 13 patients, with one or two hybrid macro-microelectrodes positioned in the insular region in each patient. Research neuropsychological paradigms could not be done in two patients for clinical reasons. In total, 23 hybrid macro-microelectrodes with 8 microcontacts each were implanted, of which 20 were recorded. Spiking activity was detected and assessed using WaveClus3. **Results**: No spiking neural activity was detected in the microcontacts of the first 7 patients. After iterative refinement during this process, successful recordings were obtained from 13 microcontacts in the anterior-inferior insula in the last four patients (13/64, 20.3%). Hybrid electrode implantation was uneventful with no complications. Obstacles included the absence of spiking activity signals, unsuccessful microwire dispersion, and the interference of environmental electrical noise on recordings. **Conclusions**: Human microelectrode recording presents a complex array of challenges; yet it holds the potential to facilitate a more comprehensive understanding of individual neuronal attributes and their specific stimulus responses.

Keywords: Microelectrode; Microcontact; Insula; Epilepsy; Single-Unit; Multi-Unit; Spike; Behnke Fried Electrode; Stereoelectroencephalography; Insular Implantation

1. Introduction

Intracranial macroelectrode implantation has proven to be a valuable neurosurgical tool in the clinical assessment of drug-resistant epilepsy. This method helps in the localization of the epileptogenic zone when non-invasive localization techniques are insufficient, and the demarcation of eloquent regions through cortical stimulation [1–3]. Intracranial electrode implantations are also great opportunities to investigate cerebral functions *in vivo* by analyzing brain responses during neuropsychological paradigms [4,5].

Various types of electrodes can be surgically inserted, either individually or in conjunction, such as subdural strip electrodes, grid electrodes, and depth electrodes for stereoelectroencephalography (SEEG). Each type of electrode can contain several *macro*-contacts, with a size of a few millimetres and capable of measuring neuronal activity from a large population of neurons [6]. In contrast, *micro*electrodes have a small contact size located at the tips of isolated wires of approximately 10-50 μm diameter. This design facilitates the delineation of extracellular action potentials from neurons [7,8] and enables the recordings of local field potentials (LFP, 1-100 Hz) at a submillimeter scale from compact neuronal clusters, as well as the action potentials emanating from sampled neurons, referred to as multi-unit activities (MUAs). After employing spike sorting techniques, it becomes possible to isolate single-unit activities (SUAs) from these recorded signals [9–12]. Moreover, microelectrode data is usually sampled at much higher frequencies (up to 40 kHz), allowing the recording of high frequency oscillations (HFOs, 80-500 Hz). However, it is important to note that due to their high impedance, microelectrodes are more susceptible to artifacts compared to macroelectrodes [12]. The predominant source of interference arises from the electrical recording environment, particularly the electrical line frequency (usually 50/60 Hz). Insufficient signal-to-noise ratio can occur if the electrical environment is excessively noisy, hindering the detection of action potentials. Hybrid depth electrodes, including macro- and microcontacts, seem to exhibit a comparable level of safety and efficacy to standard depth electrodes for intracranial monitoring, offering distinct opportunities to investigate the human brain with single-neuron resolution [13–16].

Microelectrode recordings have been a significant instrument in exploring the pathophysiology of epilepsy, particularly in understanding ictogenesis. Indeed, microelectrodes implanted within the seizure onset zone (SOZ) can record SUAs during the initiation and progression of seizures, aiding in the characterization of SOZ networks [17–19]. Additionally, microelectrodes can detect epileptic markers, including HFOs within the fast ripple band (250-500 Hz) [14,20]. Furthermore, by analyzing the waveform and firing properties of isolated neurons through spike sorting, it becomes possible to differentiate putative pyramidal cells and interneurons, providing insights into their respective contributions to seizure generation [20–22]. Finally, microelectrodes have exposed micro-seizures as distinct rhythmic events that would elude detection by macroelectrodes, owing to the enhanced resolution of microelectrodes in sampling the LFPs of significantly smaller neuronal assemblies [18,23,24]. By studying the electrical activity of neurons at a cellular level, clinicians and researchers may gain a deeper understanding of the pathological processes involved in epilepsy and develop more targeted approaches for diagnosis and treatment [25,26].

Currently, microelectrodes are implanted exclusively for research purposes in a small proportion of patients undergoing intracranial EEG evaluation, and have provided an ideal opportunity to record neuronal firing patterns in the human brain during cognitive tasks, leading to important advancements in the understanding of neuropsychological functions, such as speech encoding [27], memory encoding and retrieval [28–30], long-term and working memory [31–33], emotional processing [34,35], auditory processing [36], and face recognition [37,38]. These findings were obtained notably with microelectrodes implanted in the mesial temporal structures, including the amygdala and hippocampus, as well as in the auditory cortex, the medial frontal cortex, and the occipito-temporal junction.

Over the past decade, studies have demonstrated that a significant number of individuals with drug-resistant epilepsy who require surgery, have a suspected epileptogenic zone in the insula [1,3,39]. Due to the insula's deep location within the Sylvian fissure, surrounded by the frontal, parietal, and temporal opercula, and its proximity to other potential epileptic regions, an invasive

intracranial implantation is often necessary to confirm the involvement of the insular cortex in epileptic activity [40]. The insula is divided into two parts by the central insular sulcus: the anterior insula (aI) and the posterior insula (pI). The aI consists of three short gyri (anterior, middle, and posterior), while the pI is comprised of two long gyri (anterior and posterior) [41]. The insula has been linked to various functions, encompassing autonomic and vestibular functions, interoception, sensory processing (visceral, somatosensory, auditory, gustatory, and olfactory), as well as affective (emotion and empathy) and cognitive processes (language, attention, memory, and decision-making) [42–46].

Recordings from microelectrodes implanted in the anterior-inferior insular region offer the potential to complement traditional imaging (e.g., functional magnetic resonance imaging) and macroscale electrophysiology (i.e., electrodes with macro-contacts) by adding an additional layer of data to improve our comprehension of the complex role of the insular cortex in emotional processing and interoception. We conducted a pilot study by implanting hybrid macro-micro depth electrodes in patients with refractory epilepsy, targeting the anterior-inferior insular region. The aim of this paper is to share our experience and results with insular microelectrode recordings, describe the implantation procedure of the hybrid Behnke-Fried depth electrode and offer recommendations to improve the quality of microelectrode recordings.

2. Materials and Methods

Patients. Thirteen patients (7 females) diagnosed with refractory epilepsy underwent a multimodal evaluation and were recommended for SEEG, including insular sampling, in order to better localize the epileptogenic zone for potential surgical resection. The placement of the electrodes was determined exclusively based on clinical criteria. All patients received explanations and signed a consent form. The study was approved by the CHUM's ethical committee (#15-018) and was conducted in accordance with the ethical standards laid down in the Declaration of Helsinki. Table 1 provides descriptive characteristics of the study participants. Due to clinical reasons, patients 4 and 11 did not go through the research micro-recording process, and so only 20 out of the 23 implanted electrodes were recorded.

Table 1. List of study participants and localization of implanted electrodes.

| Patient number	Sex	No. of electrodes implanted	Localization of electrodes implanted	No. of hybrid depth electrodes and localization[1]	Surgery following implantation
1	F	17	8 R (aI, pI, amygdala, aH, pH, PCC, precuneus, cuneus) and 9 L (aI, pI, amygdala, aH, pH, PCC, precuneus/cuneus)	2 (R pI, L pI)	L temporal lobectomy
2	M	12	6 R (aI, pI, amygdala, aH, pH, OT, O) and 6 L (aI, pI, amygdala, aH, pH, OT, O)	2 (L and R aI/pI)	No surgery
3	F	14	2 R (pI, aI) and 12 L (pI, aI, P, angular, T, F, PCC)	1 (R pI)	No surgery
4	M	10	10 R (aI, pI, aH, pH, amygdala, OF, F op)	1 (R pI)	No surgery
5	M	10	10 R (aI, pI, amygdala, aH, pH, OF, ACC, PCC, median F)	2 (R aI, R pI)	No surgery
6	F	13	4 R (ACC, mesial F, OF) and 9 L (amygdala, aH, pH, OF, ACC, MCC, median F)	2 (L aI, L pI)	L temporal lobectomy
7	F	12	12 R (pI, P, ant and post precuneus, PCC, ACC, MCC)	1 (R pI)	No surgery
8	F	12	12 R (aI, pI, amygdala, pH, aH, ACC, IFG, OF, F P T op, P)	2 (R aI, R pI)	R anterior temporal lobectomy

9	F	11	1 R (aI) and 10 L (aI, pI, amygdala, aH, pH, OF, T)	2 (R aI, L pI)	No surgery
10	M	10	10 L (aI, pI, p parahippocampal, op T, fusiform, OF)	2 (L aI, L pI)	L insular lobe resection
11	M	10	10 R (aI, pI, ACC, MCC, PCC, OF, median F)	2 (R aI, R pI)	No surgery
12	F	14	8 R (aI, superior insula, T, OF, PCC, op P-T) and 6 L (aI, pI, amygdala, aH, pH, OF)	2 (R aI, L aI)	No surgery
13	M	16	16 R (aI, pI, amygdala, F op, P op, ACC, PCC, ant/mid/post median frontal, fusiform area)	2 (R aI, *R amygdala*)	R frontal corticectomy
Total		**161**		**23**	

R right, L left, aH, anterior hippocampus, pH posterior hippocampus, ACC anterior cingulate cortex, PCC posterior cingulate cortex, MCC middle cingulate cortex, F frontal, P parietal, O occipital, T temporal, OT occipito-temporal OF orbitofrontal, aI anterior insula, pI posterior insula, IFG inferior frontal gyrus, op operculum. [1]All micro contacts were localized in the anterior-inferior insula and were implanted by SEEG.

Electrophysiology. The number of macroelectrodes implanted in each patient ranged from 10 to 17, including 1 or 2 hybrid macro-microelectrodes (see Table 1). Clinical iEEG macroelectrode recordings were acquired using a Nihon-Kohden long-term monitoring system (Nihon-Kohden System, Tokyo, Japan). All macroelectrode signals were acquired continuously with Nihon-Kohden Headstages (Nihon-Kohden, Neurofax Mini Flat Junction Box, Tokyo, Japan). Microelectrode signals were recorded using a 32-channel NeuroPort system (Blackrock Microsystems, Salt Lake City, UT), with a 16-channel Cabrio Headbox connector (Ad-Tech Medical, Racine, WI). For microelectrode recordings, we used the hybrid Behnke-Fried (BF) depth electrode (Ad-Tech Medical, Racine, WI) (see Figure 1) which can record deep structures like the insula. The electrode consists of an 8-contact macro component (90-10 platinum-iridium, outer diameter 1.28 mm, length 1.57 mm) and a 9-contact micro component (90-10 platinum-iridium, outer diameter 38 μm). The micro component is covered by a protective sheath and runs through the lumen of the macro component. The macro component was used for the standard clinical recording and the micro component was used for the research recording. Eight of its microwires acted as the active recording electrodes and the 9th acted as a reference (by default but may be changed manually). The microelectrode tails were connected to the Cabrio connector. Data were recorded at 30 kHz during the experimental tasks exclusively (i.e., a few hours per day). The signal from the electrodes was high-pass filtered at 250 Hz. The implantation of hybrid electrodes proceeded without any complications.

As the procedure progressed, several materials were replaced, such as the Cabrio headbox connector (from patient #2 onwards), the shielding of all cables (from patient #8 onwards), and a preamplifier (from patient #9 and onward).
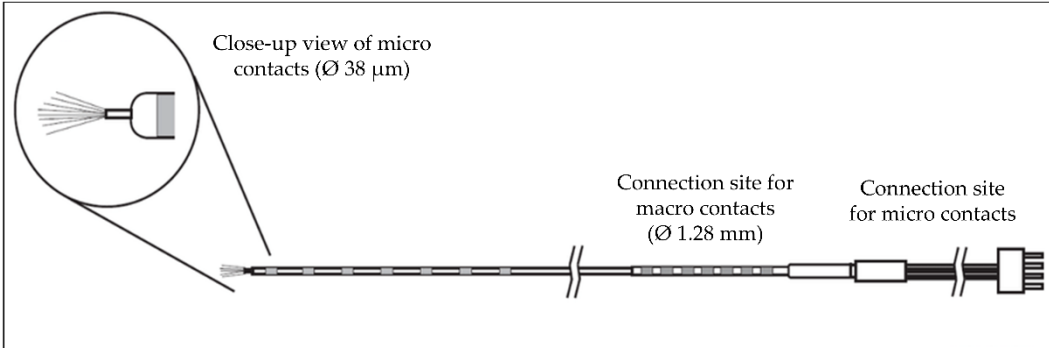

Figure 1. Schema of the Behnke-Fried electrode.

Experimental sessions. Patients were tested in their hospital room as soon as possible after SEEG implantation (an average of 3 days after surgical implantation). They were connected to both macro and microelectrode acquisition systems during the experimental tasks. A ground electrode was

placed on the left shoulder of each patient. During the first tasks, patients sat in a chair facing a laptop on which pictures were presented. In the first task, we presented pictures selected from the Nencki Affective Picture System (NAPS [47]), a standardized set of emotion eliciting color pictures (i.e., neutral, happiness, sadness, and disgust). The total task consisted of five blocks, totalling 300 stimuli, presented in a pseudorandomized order over 2000 ms with a random inter-stimulus interval (ISI) ranging from 500 to 2000 ms. Each block comprised a set of 60 pictures. The second task mirrored the first, with the additional instruction for the patient to indicate the emotion elicited by each picture. The third task involved face emotion pictures, following the same parameters as the previous tasks. In the fourth task, patients were engaged in a three-minute interoceptive task. They were first instructed to recall and re-experienced pleasant personal life events that had occurred throughout their life, such as moments of success, personal achievements, and family gatherings, and to be mindful of their bodily sensations. Subsequently, patients were instructed to recall and re-experience negative life events for three minutes. For the last two patients, we introduced two additional tasks: 1. The patients were instructed to generate highly enjoyable food imagery internally (i.e., self-generated) for three minutes; 2. The patients participated in passive listening sessions involving both pleasant and unpleasant music; each session lasted three minutes.

Preoperative planning. All patients underwent a 3T brain MRI with 3D T1+GAD and FLAIR protocol. The planning was done on a StealthStation, Medtronic Inc. Planning station. We used two optional trajectories toward the insula for single unit recording: an anterior trajectory that passes through the superior frontal gyrus and a posterior trajectory, parallel to the long insular gyri entering through the superior parietal lobule (Figure 2). Both trajectories ended in the antero-inferior corner of the insula. Fine trajectory adjustments were done to assure a safe distance from blood vessels. Because microwires protrude beyond the distal end of the macroelectrode, we made sure there was 5 mm of insular cortex post-target as well.
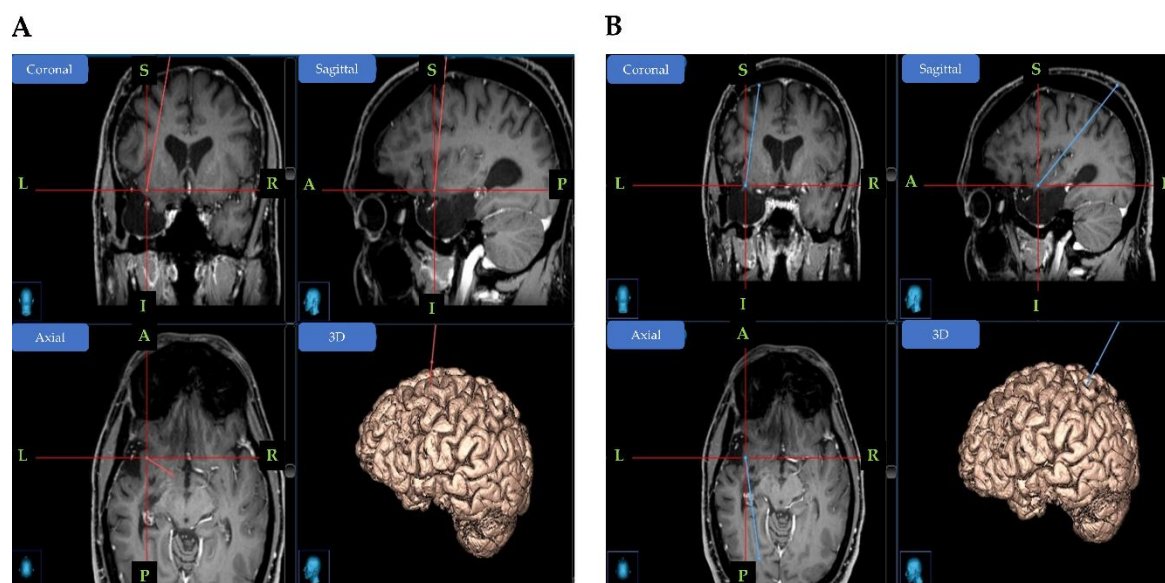
Figure 2. Example of the preoperative planning. **A**: Hybrid electrode implanted in the left anterior insula (anterior trajectory), and **B**; Hybrid electrode implanted in the left posterior insula (posterior trajectory). R: right; L; left; A: anterior; P: posterior; S: superior; I: inferior.

Operative procedure. The patient was brought into the operating room (OR) where they underwent general anesthesia and endotracheal intubation. The patient's head was completely shaved and local anesthesia (xylazine and bupivacaine) was injected to the four skull pin sites. A stereotactic frame (CRW, Integra Inc.) was placed, and the patient was transferred to the computed tomography (CT) scan suit. A stereotactic localizer was placed on the frame and the patient underwent a head CT scan (axial images, 1 mm slice thickness). The localizer was removed and the patient was taken back to the OR. The scan images were transferred to the planning computer and

merged with the previously acquired MRI images. The x, y, z coordinates and the trajectory angles for each of the targets were defined. The bone thickness was calculated on the planning computer for each of the trajectories.

The patient was positioned supine on the operating table with the CRW frame fixed to the Mayfield head holder. Their head was entirely prepped with antiseptic solution and covered by an incise drape. The stereotactic head frame was assembled on the CRW base ring and secured with three locking knobs. Two sterile drapes were draped around the head frame to create a sterile field. The coordinates and angles were set on the stereotactic frame and double checked by two neurosurgeons. A reducing tube was inserted through a guide block on the frame and the exact entry point on the skin was marked. A 0.5 cm skin incision was performed down to the skull and hemostasis was achieved using bipolar cautery if needed.

A twist drill was inserted through the reducing tube down to the skull. A drill stopper was set to a distance of 5 mm plus the calculated bone thickness, in order to ensure piercing the dura matter. A hex wrench with anchor bolt was inserted through the reducing tube into the drilled hole. The anchor bolt was screwed until a significant increase in resistance was felt. The distance between the target and the external edge of the guide block was 170 mm. The length of the k-wire was measured on a metal ruler and marked at 150 mm from its distal tip. This causes the k-wire to stop 20 mm before the target to minimize the risk of deep vascular injury. The macro component of the BF electrode was measured as well and marked at 170 mm from its distal tip. The microwires at the distal tip of the BF micro component were cut diagonally to a length of 3-5 mm using sharp scissors. The microwires were separated from each other using gentle finger movements. The green sheath was pulled over the microwires. The K-wire was slowly inserted through the anchor bolt until the marked point aligns with the external part of the block guide and then pulled back. The assembled micro-macro BF electrode was then inserted in the same way until reaching the marked depth. The electrode stylet was removed and the anchor bolt screw tightened. The same procedure was repeated for the rest of the electrodes. The entire head was cleaned and the frame removed. A full head dressing was applied, the patient was awakened and taken to the recovery room. After a night of observation in an intermediate care unit, a 3D T1 + FLAIR head MRI was performed and the patient was transferred to the EEG monitoring unit.

Post-implant monitoring. The anatomical locations of the electrodes were routinely verified after the implantation by MRI coregistered to the preoperative MRI. Special attention was taken to ensure that the distal end of the metallic artifact was located in the insular cortex. In addition, by advancing the marker on the planning station a few millimeters further on the same trajectory, we confirmed the presence of cortex where the microwires were supposed to be located. Following implantation, the electrodes were carefully covered with a bandage, forming a 'headwrap', ensuring their protection.

Electrode removal. After completing the monitoring period, the electrodes were removed. If immediate resective surgery was planned, the electrodes were removed under general anesthesia just prior to surgery. Otherwise, the electrodes were removed at bedside in the EEG monitoring unit. After meticulous disinfection of the electrode entry sites, the anchor bolts were released and the electrodes were gently pulled out. A surgical staple was placed at each electrode site to prevent CSF leakage through the skin incision.

Spike extraction and experimental analysis. For the 4 patients from whom we obtained usable microcontact data, spike detection and sorting were performed on each microcontact separately using the WaveClus3 open source spike sorting tool [48], which is well-established and commonly used in the field. Within WaveClus3, each channel's signal (recorded at 30 kHz sampling rate) first goes through a second order elliptic filter ranging between 300 Hz and 3000 Hz, with the low-frequency and high-frequency cutoffs chosen to reduce low-frequency drift and high-frequency noise respectively, while maintaining the signal in the range relevant for spikes. Next, spikes are detected using an amplitude threshold, defined as a multiple of the recording's noise level, and a brief refractory period, assuring each spike is only detected once. These parameters can be changed manually, but we used the default values of a multiple of 5 for the amplitude threshold and the

default refractory period, set as 1.5 ms. Based on visual verification of our spike-sample, we used a threshold type of "neg", meaning only negative crossings of the threshold are considered for the detection.

After their detection, the goal is to assign each detected spike to one of a few clusters consisting of spikes either from an isolated single neuron or from a small group of multiple-neurons. For this, the detected spikes are transformed using wavelet decomposition to compactly represent their structural and temporal features while suppressing noise. Then, using Superparamagnetic Clustering (SPC) [49] the spikes are grouped based on these features, such that each cluster is regarded as originating from a distinct unit or multi-unit group. This idea relies on the principle that a recorded spike's shape and temporal properties are mostly influenced by the structural and spatial properties of its source [50]. SPC is an unsupervised process derived from the field of statistical mechanics. It groups data points based on their pairwise similarities according to a "temperature" variable, which determines the similarity level required to group data points to the same cluster. The higher the temperature is, the lower the similarity required between data points to belong to the same cluster. The SPC process is performed with different temperature values, and the final clusters are chosen based on a threshold that considers how their size changes as the temperature changes.

3. Results

Table 1 provides a summary of the recordings. In total, 20 hybrid macro-microelectrodes were implanted and recorded from in the anterior-inferior insular region across 11 patients with refractory epilepsy, totalling 160 microcontacts (8 microcontacts per electrode). In the first 7 patients, the recorded data were compromised by 60 Hz line-noise contamination and lacked detectable neuronal activity.

In the final 4 recorded patients, after equipment replacement and improved shielding, the 60 Hz artifact was no longer an issue. We recorded activity from 64 microcontacts (channels) across 8 electrodes from these patients. By visual inspection, we detected spiking activity in 13 of these channels (13/64 = 20.3%; Table 2). We then passed the signal from each channel to WaveClus3, with a negative detection threshold setting of 5 times the standard deviation. We isolated 12 clusters which correspond to the putative single-unit activity of 12 separate neurons, and 21 additional clusters corresponding to the putative multi-unit activity of 21 multi-neuron groups. Figure 3 shows an example of the spikes detected in one of the microcontacts, separated into clusters using the WaveClus3 algorithm. In this particular contact, 3 distinct single units were obtained.

Table 2. Summary of single-unit clusters and putative multi-unit clusters for each of the last 4 recorded participants.

Patients[1]	duration of recording (min:sec)	No. of microcontacts[2] with neuronal activity	No. of well isolated units	No. of putative multi units detected
9	05:08	2/16	1	3
10	24:25	6/16	6	9
12	14:40	3/16	4	6
13	03:57	2/16	1	3
		13/64 (20.3%)	**12**	**21**

[1] Patient #11 not recorded. [2] All micro contacts were localized in the anterior-inferior insula and were implanted by SEEG.
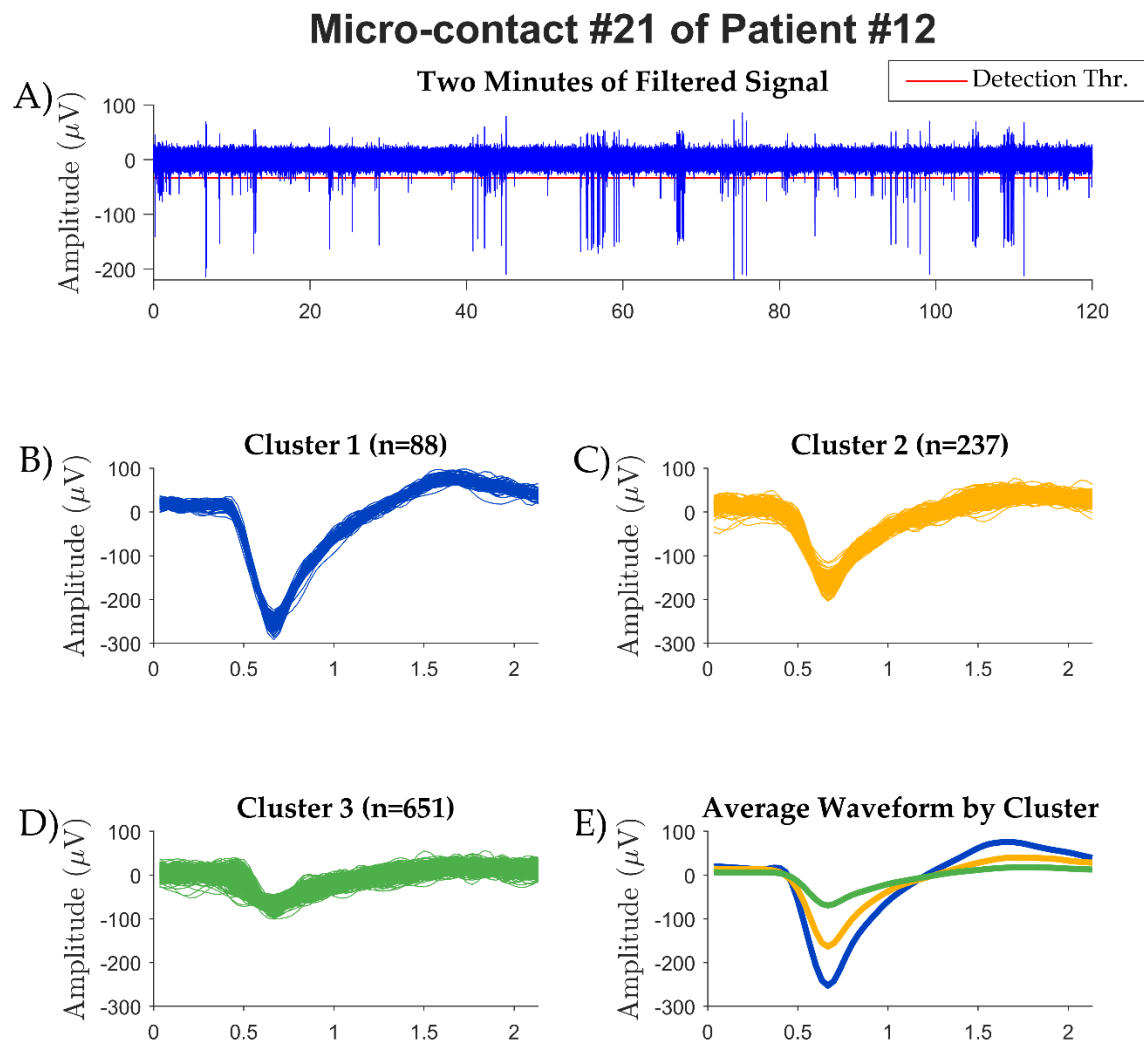
Figure 3. An example of data from a microcontact and its analysis with WaveClus. **A)** The first 2 minutes recorded from one of the microelectrodes after being filtered. The threshold amplitude used by WaveClus for spike detection is marked in Red **B)-D**) The three clusters with well-isolated single units returned from the WaveClus3 algorithm. For each cluster, all the spikes belonging to it are superimposed on each other. The number of spikes assigned to each cluster is provided in the sub-title as n. **E)** The average spike shapes of each single unit cluster, each identified by a different color (Blue for cluster 1, Yellow for cluster 2, Green for cluster 3).

We characterized single units using standard metrics [51] and tabulate them in Table 3. Across all single units, the average spike width, measured as the trough-to-peak duration, was 1.07 ± 0.09 ms (mean$\pm$standard-deviation; Figure 4). The peak signal-to-noise ratio (SNR), calculated as the ratio between the trough-to-peak amplitude and the standard-deviation of the background noise (as estimated by WaveClus [52], was 5.56 ± 2.65. The mean firing rate across all single units was 1.66 ± 3.07 Hz. The percentage of inter spike intervals (ISIs) which were lower than 3 ms was $0.22 \pm 0.4\%$, with a median of 0%. These firing-rate and ISI percentage (below 3 ms) values are plotted along with those for multi-units in Figure 5. The mean modified coefficient of variation in the ISI (commonly referred to as CV2 [53]) was 1.1 ± 0.14, and not significantly different from 1 (the value for a Poisson process).

Table 3. Metrics for each well-isolated single unit.

| Unit ID	Average firing rate (Hz)	Average spike width (ms)	% intervals below 3 ms	Trough to Peak SNR	CV2
1	0.22	1.03	0	5.87	1.1
2	9.24	0.93	1.38%	3.82	1
3	6.99	0.97	0.41%	4.32	0.8
4	0.65	1.03	0	5.62	1
5	0.16	1.20	0	7.33	1.2
6	0.19	1.23	0	3.87	1.3
7	0.09	1.07	0	6.22	1.2
8	0.76	1.17	0.30%	2.93	1.1
9	0.27	1.03	0.42%	7.64	1.2
10	0.74	1.07	0.15%	3.27	1.1
11	0.1	1.00	0	12.33	1.2
12	0.46	1.07	0	3.55	1.1
mean	**1.66**	**1.07**	**0.22**	**5.56**	**1.10**
median	**0.3**	**1.05**	**0.00**	**4.97**	**1.1**
SD	**3.07**	**0.09**	**0.00**	**2.65**	**0.14**
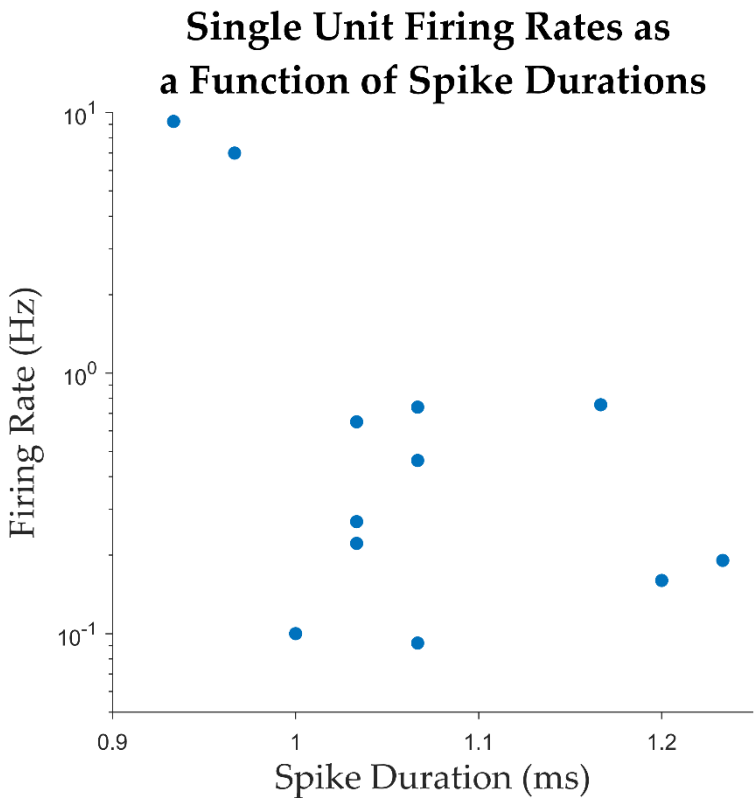
Figure 4. Average firing rates plotted against spike durations. Each dot in the plot corresponds to one single unit detected.

Average Firing Rate and ISI % Under 3 ms Over All Clusters
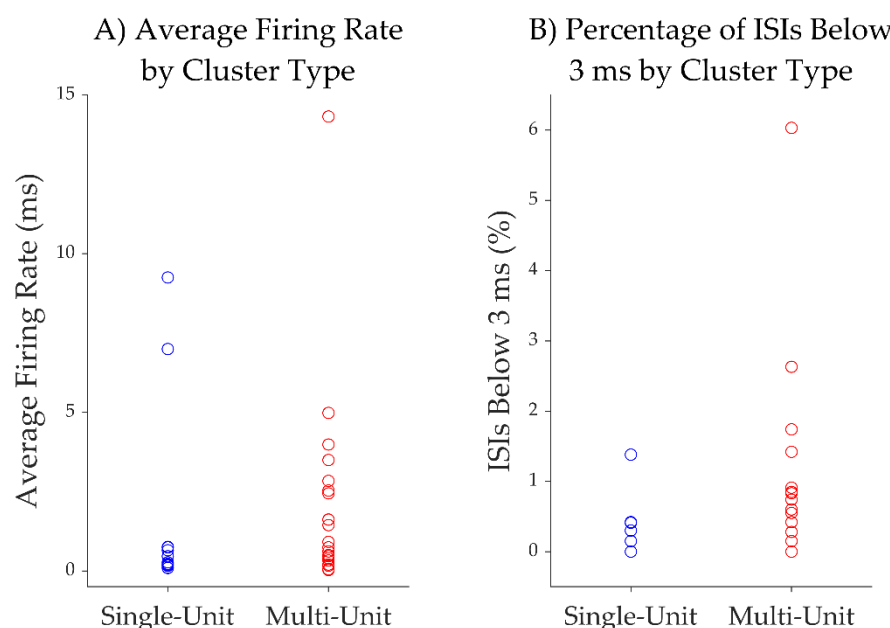
Figure 5. A) Average firing rate of clusters, separated to single-unit and multi-unit clusters. **B)** The percentage of ISIs below 3 ms for each cluster, separated into single-unit and multi-unit clusters.

4. Discussion

As anticipated, the endeavor to obtain unit recordings and local field potentials using microelectrodes in the clinical environment presented certain challenges. These challenges encompassed the absence of discernible neuronal activity signals, unsuccessful dispersion of microwires, and contamination of recordings due to environmental electrical noise. After several attempts, successful recordings of neural activity from isolated neurons were accomplished during our neuropsychological tasks.

Following the implantation of hybrid macro-microelectrodes, the recordings during experimental tasks posed inherent challenges that need to be addressed. Obstacles encompassed the absence of neuronal activity signals, interference of environmental electrical noise, artifacts caused by the reference and ground choices, and unsuccessful microwire dispersion.

Absence of Neuronal Activity Signals:

During the patients' stay at the epilepsy unit monitoring, we encountered limitations in recording the complete neuronal activity using our Cabrio headbox 16-channel system. Despite having implanted electrodes in the relevant regions, certain channels exhibited a constant lack of detectable neural signal. We propose that this issue may have resulted from breaks in the microwires caused by excessive tensile forces during various physical manipulations, such as headwrap changes, surgery, initial hook-up, and so on. Moreover, it is important to note that placing microwires in a region with a thin layer of grey matter (usually less than 5 mm) such as the insula can result in a lower yield of recorded neurons [54]. Despite technically successful implantations without any observed failure modes, certain microwires failed to record any neuronal units. We postulate that these specific microwires were not positioned in close proximity to active cells.

Power Line Interference Issue:

Power line contamination is a term used to describe electromagnetic interference that occurs at frequencies of 50/60 Hz, which originates from power lines or external sources of voltage. This interference generates an electric field with the capability to produce coupled currents in conductors that lack shielding. As a consequence, this leads to the occurrence of an extra alternating voltage in recorded data [55]. In a hospital setting, it is crucial to acknowledge that various equipment and

personal electronic devices can emit electromagnetic radiation (e.g., beds, chair, lights, monitors, cables, etc.). Furthermore, it is important to recognize that both the patient and the components of the recording system, including the electrodes and connecting cables, can function as antennas in this environment. During our initial recordings, we frequently encountered data contamination caused by electromagnetic interference, rendering the recorded data unusable. To address this issue, we implemented shielding measures for the cable connecting the 16-channel headstages to the amplifier, employing aluminium foil to create a shielding effect similar to a Faraday cage around the recording cables. The implementation of this shielding technique significantly improved the quality of our data. Nevertheless, even when operating on battery power, a laptop can introduce interference for the microelectrodes if the patient interacts with the keyboard (it was the case during our active experimental tasks). A viable solution, particularly for cognitive tasks that require responses, involves employing optical cables to connect to button response boxes, or wireless keyboards and/or mice, as suggested by Lehongre and colleagues [56].

Artifacts: Reference and Ground

The choice of reference electrode for microelectrode recordings is a crucial consideration. This reference electrode serves as a baseline for measuring the electrical activity of the target neurons. It should ideally have a stable and low impedance, share as much of the common noise in the signal electrodes as possible, as well as have a minimal independent contribution to the overall noise in the recording [54]. When selecting the reference electrode for microcontacts recordings, several factors need to be considered. Firstly, one important factor is the proximity of the reference electrode to the recording site (i.e., to have the reference electrode as close as possible to the target neurons to minimize the introduction of additional noise). Secondly, one needs to consider the type of reference electrode used. In general, common choices include large surface electrodes (i.e., applied to the skin of the subject), microelectrodes, or a combination of both. Large surface electrodes provide a low-impedance reference but may introduce additional noise due to their larger size. On the other hand, microcontact can match the geometry and impedance of the recording sites but may have higher impedance and contribute more thermal noise to the recordings [8,57,58]. In our experiments, we made several attempts to mitigate artifacts caused by the selection of the reference electrode. From our seventh recorded patient, it was determined that using the ninth microwire of our microelectrode was a more advantageous option compared to using an electrode on the mastoid. This optimization of the reference electrode placement significantly enhanced the quality of our microelectrode recordings afterwards. On the other hand, the ground electrode was strategically placed in a neutral region, specifically on the shoulder of our patients, to ensure a significant distance from any potential electrical interference sources.

Unsuccessful microwire dispersion:

Our post-implantation imaging analysis revealed that some microelectrodes were in grey matter as expected, but some were in white matter, partly explaining our difficulty to record neuronal activity. Moreover, in our first two cases, we noticed that in some BF electrodes, the microwires were stuck together as a bundle. As this can be a cause for recording failure, we adjusted the implantation method and made sure to spread the wires with gentle finger movement before inserting them. Figure 6 showed suboptimal (a) and optimal (b) wires spread as seen post removal.
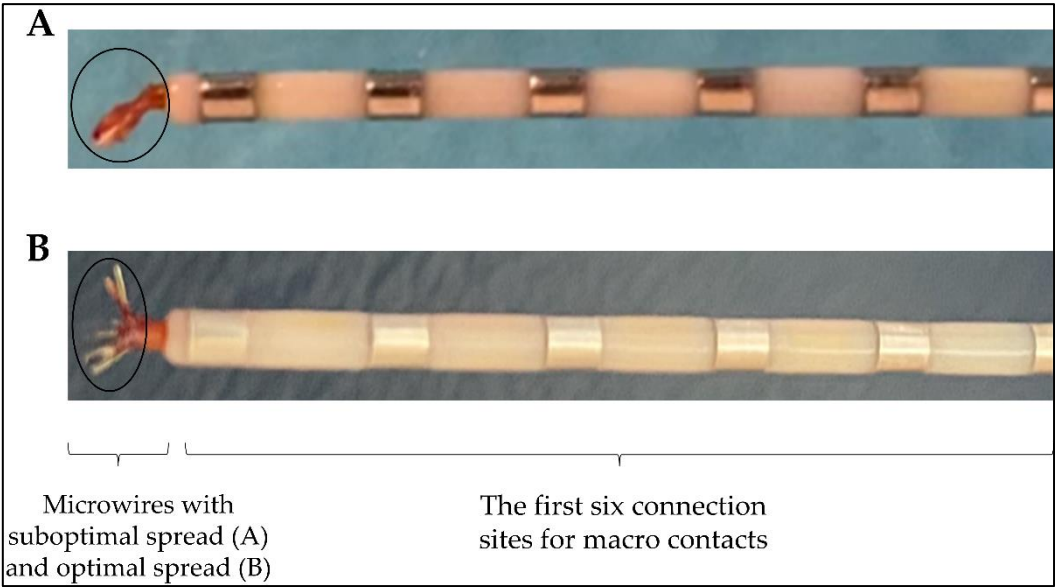
Figure 6. Microwires of Behnke-Fried electrodes: **(A)** suboptimal; **(A)** optimal.

Successful recordings:

After troubleshooting over the first seven unsuccessful recording process, our procedures reliably yielded successful recordings of both single neurons and multi-unit clusters in the most recent four patients in our series. We have outlined our troubleshooting steps above so that they can be helpful to guide similar efforts by others. The statistics of our isolated single-units from the insula roughly match those reported in the literature for similar recordings from the human hippocampus, despite using different spike detection methods [51]. Our ongoing recordings will enable more detailed characterization of the properties of insular neurons in the context of various neuropsychological tasks and also enable more detailed comparisons with other datasets as well as our own recordings from non-insular areas. Main recommendations are presented in Table 4 as a guide.

Table 4. Summary of guidelines.

	Encountered difficulties	Recommendations
Implantation surgery	Microwires bundled	Spread the wires before insertion. Check the spread wires in the MRI post-implantation.
	Hybrid electrode trajectories	Prior to the insertion of microelectrodes into the macroelectrodes, microwires must be cut to the desired length defined during the planning surgery.
Post-implantation surgery	Hybrid electrodes without microcontact signal	Do not bend and/or pull the cables of the electrodes. Test the patient as soon as possible following the surgery implantation. Confirm the localization of the microcontacts in the grey or white matter.
Testing	Power line contamination	Use shielded cables, aluminum foils. Unplug all devices in the room of the patient. Use a power conditioner for laptop, optical cable and/or wireless. No cellphone in the room.
	Artifacts	Check the reference electrode and the ground. Stabilize the Cabrio connector, headstage and cables. Minimize movements by the patient. All connector cables in the same direction.

5. Conclusions

This study showed that it is feasible to record insular microelectrode signals *in vivo* in patients with epilepsy. We propose in detail several technical guidelines to enable the successful implantation and the recording of hybrid macro-microelectrodes in the human insular cortex. Although insular cortex human microelectrode recording presents a complex array of challenges, this methodology may allow for notable advancements in our understanding of the role and functions of specific subregions of the insula.

Author Contributions: Conceptualization, D.C., O.B. and D.K.N.; methodology, D.C., O.B. and D.K.N.; software, S.K., M.A. and K.J.; implantation, S.H. and A.B.; data acquisition, D.C. and M.R.; formal analysis, S.K., M.A. and K.J.; writing—original draft preparation, D.C., S.H., S.K., M.A., K.J. and D.K.N.; writing—review and editing, D.C., S.H., S.K., M.A., K.J., A.B., M.R., O.B. and D.K.N; supervision, O.B., S.K. and D.K.N.; funding acquisition, O.B. and D.K.N. All authors have read and agreed to the published version of the manuscript.

Institutional Review Board Statement: The study was conducted in accordance with the Declaration of Helsinki and approved by the Ethics Committee of the CHUM (15-018; June 2015).

Informed Consent Statement: Informed consent was obtained from all subjects involved in the study.

Data Availability Statement: Not applicable.

Conflicts of Interest: The authors declare no conflicts of interest.

References

1. Isnard, J.; Guenot, M.; Sindou, M.; Mauguiere, F., Clinical manifestations of insular lobe seizures: a stereo-electroencephalographic study. *Epilepsia* **2004,** *45* (9), 1079-90.

2. Mazzola, L.; Mauguiere, F.; Isnard, J., Electrical Stimulations of the Human Insula: Their Contribution to the Ictal Semiology of Insular Seizures. *J Clin Neurophysiol* **2017,** *34* (4), 307-314.

3. Nguyen, D. K.; Nguyen, D. B.; Malak, R.; Leroux, J. M.; Carmant, L.; Saint-Hilaire, J. M.; Giard, N.; Cossette, P.; Bouthillier, A., Revisiting the role of the insula in refractory partial epilepsy. *Epilepsia* **2009,** *50* (3), 510-20.

4. Citherlet, D.; Boucher, O.; Tremblay, J.; Robert, M.; Gallagher, A.; Bouthillier, A.; Lepore, F.; Nguyen, D. K., Spatiotemporal dynamics of auditory information processing in the insular cortex: an intracranial EEG study using an oddball paradigm. *Brain Struct Funct* **2020,** *225* (5), 1537-1559.

5. Llorens, A.; Bellier, L.; Blenkmann, A. O.; Ivanovic, J.; Larsson, P. G.; Lin, J. J.; Endestad, T.; Solbakk, A. K.; Knight, R. T., Decision and response monitoring during working memory are sequentially represented in the human insula. *iScience* **2023,** *26* (10), 107653.

6. Parvizi, J.; Kastner, S., Promises and limitations of human intracranial electroencephalography. *Nat Neurosci* **2018,** *21* (4), 474-483.

7. Chari, A.; Thornton, R. C.; Tisdall, M. M.; Scott, R. C., Microelectrode recordings in human epilepsy: a case for clinical translation. *Brain Commun* **2020,** *2* (2), fcaa082.

8. Prasad, A.; Sanchez, J. C., Quantifying long-term microelectrode array functionality using chronic in vivo impedance testing. *J Neural Eng* **2012,** *9* (2), 026028.

9. Harris, K. D.; Quiroga, R. Q.; Freeman, J.; Smith, S. L., Improving data quality in neuronal population recordings. *Nat Neurosci* **2016,** *19* (9), 1165-74.

10. Mukamel, R.; Fried, I., Human intracranial recordings and cognitive neuroscience. *Annu Rev Psychol* **2012,** *63*, 511-37.

11. Pedreira, C.; Martinez, J.; Ison, M. J.; Quiroga, R. Q., How many neurons can we see with current spike sorting algorithms? *J Journal of neuroscience methods* **2012,** *211* (1), 58-65.

12. Stacey, W. C.; Kellis, S.; Greger, B.; Butson, C. R.; Patel, P. R.; Assaf, T.; Mihaylova, T.; Glynn, S., Potential for unreliable interpretation of EEG recorded with microelectrodes. *Epilepsia* **2013,** *54* (8), 1391-401.

13. Carlson, A. A.; Rutishauser, U.; Mamelak, A. N., Safety and Utility of Hybrid Depth Electrodes for Seizure Localization and Single-Unit Neuronal Recording. *Stereotact Funct Neurosurg* **2018,** *96* (5), 311-319.

14. Khoo, H. M.; Hall, J. A.; Dubeau, F.; Tani, N.; Oshino, S.; Fujita, Y.; Gotman, J.; Kishima, H., Technical Aspects of SEEG and Its Interpretation in the Delineation of the Epileptogenic Zone. *Neurol Med Chir (Tokyo)* **2020,** *60* (12), 565-580.

15. Misra, A.; Burke, J. F.; Ramayya, A. G.; Jacobs, J.; Sperling, M. R.; Moxon, K. A.; Kahana, M. J.; Evans, J. J.; Sharan, A. D., Methods for implantation of micro-wire bundles and optimization of single/multi-unit recordings from human mesial temporal lobe. *J Neural Eng* **2014,** *11* (2), 026013.

16. Tay, A. S.-M. S.; Caravan, B.; Mamelak, A. N., Which Are the Most Important Aspects of Microelectrode Implantation? In *Intracranial EEG*, Axmacher, N., Ed. Springer International Publishing: Cham, 2023; pp 671-682.

17. Lambrecq, V.; Lehongre, K.; Adam, C.; Frazzini, V.; Mathon, B.; Clemenceau, S.; Hasboun, D.; Charpier, S.; Baulac, M.; Navarro, V.; Le Van Quyen, M., Single-unit activities during the transition to seizures in deep mesial structures. *Ann Neurol* **2017,** *82* (6), 1022-1028.

18. Schevon, C. A.; Ng, S. K.; Cappell, J.; Goodman, R. R.; McKhann, G., Jr.; Waziri, A.; Branner, A.; Sosunov, A.; Schroeder, C. E.; Emerson, R. G., Microphysiology of epileptiform activity in human neocortex. *J Clin Neurophysiol* **2008,** *25* (6), 321-30.

19. Schevon, C. A.; Weiss, S. A.; McKhann, G., Jr.; Goodman, R. R.; Yuste, R.; Emerson, R. G.; Trevelyan, A. J., Evidence of an inhibitory restraint of seizure activity in humans. *Nat Commun* **2012,** *3* (1), 1060.

20. Weiss, S. A.; Alvarado-Rojas, C.; Bragin, A.; Behnke, E.; Fields, T.; Fried, I.; Engel, J., Jr.; Staba, R., Ictal onset patterns of local field potentials, high frequency oscillations, and unit activity in human mesial temporal lobe epilepsy. *Epilepsia* **2016,** *57* (1), 111-21.

21. Elahian, B.; Lado, N. E.; Mankin, E.; Vangala, S.; Misra, A.; Moxon, K.; Fried, I.; Sharan, A.; Yeasin, M.; Staba, R.; Bragin, A.; Avoli, M.; Sperling, M. R.; Engel, J., Jr.; Weiss, S. A., Low-voltage fast seizures in humans begin with increased interneuron firing. *Ann Neurol* **2018,** *84* (4), 588-600.

22. Truccolo, W.; Donoghue, J. A.; Hochberg, L. R.; Eskandar, E. N.; Madsen, J. R.; Anderson, W. S.; Brown, E. N.; Halgren, E.; Cash, S. S., Single-neuron dynamics in human focal epilepsy. *Nat Neurosci* **2011,** *14* (5), 635-41.

23. Staba, R. J.; Wilson, C. L.; Bragin, A.; Fried, I.; Engel, J., Jr., Quantitative analysis of high-frequency oscillations (80-500 Hz) recorded in human epileptic hippocampus and entorhinal cortex. *J Neurophysiol* **2002,** *88* (4), 1743-52.

24. Stead, M.; Bower, M.; Brinkmann, B. H.; Lee, K.; Marsh, W. R.; Meyer, F. B.; Litt, B.; Van Gompel, J.; Worrell, G. A., Microseizures and the spatiotemporal scales of human partial epilepsy. *Brain* **2010,** *133* (9), 2789-97.

25. Engel, A. K.; Moll, C. K.; Fried, I.; Ojemann, G. A., Invasive recordings from the human brain: clinical insights and beyond. *Nat Rev Neurosci* **2005,** *6* (1), 35-47.

26. Park, Y. S.; Cosgrove, G. R.; Madsen, J. R.; Eskandar, E. N.; Hochberg, L. R.; Cash, S. S.; Truccolo, W., Early Detection of Human Epileptic Seizures Based on Intracortical Microelectrode Array Signals. *IEEE Trans Biomed Eng* **2020,** *67* (3), 817-831.

27. Chan, A. M.; Dykstra, A. R.; Jayaram, V.; Leonard, M. K.; Travis, K. E.; Gygi, B.; Baker, J. M.; Eskandar, E.; Hochberg, L. R.; Halgren, E.; Cash, S. S., Speech-specific tuning of neurons in human superior temporal gyrus. *Cereb Cortex* **2014,** *24* (10), 2679-93.

28. Ison, M. J.; Quian Quiroga, R.; Fried, I., Rapid Encoding of New Memories by Individual Neurons in the Human Brain. *Neuron* **2015,** *87* (1), 220-30.

29. Kucewicz, M. T.; Michael Berry, B.; Bower, M. R.; Cimbalnik, J.; Svehlik, V.; Matt Stead, S.; Worrell, G. A., Combined Single Neuron Unit Activity and Local Field Potential Oscillations in a Human Visual Recognition Memory Task. *IEEE Trans Biomed Eng* **2016,** *63* (1), 67-75.

30. Quiroga, R. Q., Concept cells: the building blocks of declarative memory functions. *Nat Rev Neurosci* **2012,** *13* (8), 587-97.

31. Kamiński, J.; Sullivan, S.; Chung, J. M.; Ross, I. B.; Mamelak, A. N.; Rutishauser, U., Persistently active neurons in human medial frontal and medial temporal lobe support working memory. *J Nature neuroscience* **2017,** *20* (4), 590-601.

32. Rutishauser, U.; Reddy, L.; Mormann, F.; Sarnthein, J., The Architecture of Human Memory: Insights from Human Single-Neuron Recordings. *J Neurosci* **2021,** *41* (5), 883-890.

33. Rutishauser, U.; Ross, I. B.; Mamelak, A. N.; Schuman, E. M., Human memory strength is predicted by theta-frequency phase-locking of single neurons. *Nature* **2010,** *464* (7290), 903-7.

34. Wang, S.; Tudusciuc, O.; Mamelak, A. N.; Ross, I. B.; Adolphs, R.; Rutishauser, U., Neurons in the human amygdala selective for perceived emotion. *Proc Natl Acad Sci U S A* **2014,** *111* (30), E3110-9.

35. Wang, S.; Yu, R.; Tyszka, J. M.; Zhen, S.; Kovach, C.; Sun, S.; Huang, Y.; Hurlemann, R.; Ross, I. B.; Chung, J. M.; Mamelak, A. N.; Adolphs, R.; Rutishauser, U., The human amygdala parametrically encodes the intensity of specific facial emotions and their categorical ambiguity. *Nat Commun* **2017,** *8* (1), 14821.

36. Bitterman, Y.; Mukamel, R.; Malach, R.; Fried, I.; Nelken, I., Ultra-fine frequency tuning revealed in single neurons of human auditory cortex. *Nature* **2008,** *451* (7175), 197-201.

37. Decramer, T.; Premereur, E.; Zhu, Q.; Van Paesschen, W.; van Loon, J.; Vanduffel, W.; Taubert, J.; Janssen, P.; Theys, T., Single-Unit Recordings Reveal the Selectivity of a Human Face Area. *J Neurosci* **2021,** *41* (45), 9340-9349.

38. Mormann, F.; Niediek, J.; Tudusciuc, O.; Quesada, C. M.; Coenen, V. A.; Elger, C. E.; Adolphs, R., Neurons in the human amygdala encode face identity, but not gaze direction. *Nat Neurosci* **2015,** *18* (11), 1568-70.

39. Obaid, S.; Zerouali, Y.; Nguyen, D. K., Insular Epilepsy: Semiology and Noninvasive Investigations. *J Clin Neurophysiol* **2017,** *34* (4), 315-323.

40. Surbeck, W.; Bouthillier, A.; Weil, A. G.; Crevier, L.; Carmant, L.; Lortie, A.; Major, P.; Nguyen, D. K., The combination of subdural and depth electrodes for intracranial EEG investigation of suspected insular (perisylvian) epilepsy. *Epilepsia* **2011,** *52* (3), 458-66.

41. Ture, U.; Yasargil, D. C.; Al-Mefty, O.; Yasargil, M. G., Topographic anatomy of the insular region. *J Neurosurg* **1999,** *90* (4), 720-33.

42. Gogolla, N., The insular cortex. *Curr Biol* **2017,** *27* (12), R580-R586.

43. Uddin, L. Q.; Nomi, J. S.; Hebert-Seropian, B.; Ghaziri, J.; Boucher, O., Structure and Function of the Human Insula. *J Clin Neurophysiol* **2017,** *34* (4), 300-306.

44. Lamm, C.; Singer, T., The role of anterior insular cortex in social emotions. *Brain Struct Funct* **2010,** *214* (5-6), 579-91.

45. Shura, R. D.; Hurley, R. A.; Taber, K. H., Insular cortex: structural and functional neuroanatomy. *J Neuropsychiatry Clin Neurosci* **2014,** *26* (4), 276-82.

46. Uddin, L. Q.; Kinnison, J.; Pessoa, L.; Anderson, M. L., Beyond the tripartite cognition-emotion-interoception model of the human insular cortex. *J Cogn Neurosci* **2014,** *26* (1), 16-27.

47. Marchewka, A.; Zurawski, L.; Jednorog, K.; Grabowska, A., The Nencki Affective Picture System (NAPS): introduction to a novel, standardized, wide-range, high-quality, realistic picture database. *Behav Res Methods* **2014,** *46* (2), 596-610.

48. Chaure, F. J.; Rey, H. G.; Quian Quiroga, R., A novel and fully automatic spike-sorting implementation with variable number of features. *J Neurophysiol* **2018,** *120* (4), 1859-1871.

49. Gold, C.; Henze, D. A.; Koch, C.; Buzsaki, G., On the origin of the extracellular action potential waveform: A modeling study. *J Neurophysiol* **2006,** *95* (5), 3113-28.

50. Blatt, M.; Wiseman, S.; Domany, E., Superparamagnetic clustering of data. *Phys Rev Lett* **1996,** *76* (18), 3251-3254.

51. Faraut, M. C. M.; Carlson, A. A.; Sullivan, S.; Tudusciuc, O.; Ross, I.; Reed, C. M.; Chung, J. M.; Mamelak, A. N.; Rutishauser, U., Dataset of human medial temporal lobe single neuron activity during declarative memory encoding and recognition. *Sci Data* **2018,** *5* (1), 180010.

52. Quiroga, R. Q.; Nadasdy, Z.; Ben-Shaul, Y., Unsupervised spike detection and sorting with wavelets and superparamagnetic clustering. *Neural Comput* **2004,** *16* (8), 1661-87.

53. Holt, G. R.; Softky, W. R.; Koch, C.; Douglas, R. J., Comparison of discharge variability in vitro and in vivo in cat visual cortex neurons. *J Neurophysiol* **1996,** *75* (5), 1806-14.

54. Afif, A.; Chabardes, S.; Minotti, L.; Kahane, P.; Hoffmann, D., Safety and usefulness of insular depth electrodes implanted via an oblique approach in patients with epilepsy. *Neurosurgery* **2008,** *62* (5 Suppl 2), ONS471-9; discussion 479-80.

55. Mateo, J.; Sánchez-Morla, E. M.; Santos, J. L., A new method for removal of powerline interference in ECG and EEG recordings. *Comput Electr Eng* **2015,** *45*, 235-248.

56. Lehongre, K.; Lambrecq, V.; Whitmarsh, S.; Frazzini, V.; Cousyn, L.; Soleil, D.; Fernandez-Vidal, S.; Mathon, B.; Houot, M.; Lemarechal, J. D.; Clemenceau, S.; Hasboun, D.; Adam, C.; Navarro, V., Long-term deep intracerebral microelectrode recordings in patients with drug-resistant epilepsy: Proposed guidelines based on 10-year experience. *Neuroimage* **2022,** *254*, 119116.

57. Ludwig, K. A.; Miriani, R. M.; Langhals, N. B.; Joseph, M. D.; Anderson, D. J.; Kipke, D. R., Using a common average reference to improve cortical neuron recordings from microelectrode arrays. *J Neurophysiol* **2009,** *101* (3), 1679-89.

58. Banstola, A.; Silva, C.; Ulrich, K.; Ruan, M.; Robertson, L.; McNaughton, N., Construction of simple, customised, brain-spanning, multi-channel, linear microelectrode arrays. *J Neurosci Methods* **2021,** *348*, 109011.